Plant Communications
Research article

CellPress
Partner Journal

Loss of the accessory chromosome converts a pathogenic tree-root fungus into a mutualistic endophyte

Huanshen Wei[1,2,8], Zhenhui Zhong[3,8], Zhongfeng Li[1,2,8], Yuwei Zhang[1,2,8], Eva H. Stukenbrock[4,5,*], Boping Tang[6], Ningning Yang[1,2], Riccardo Baroncelli[7], Long Peng[1,2], Zhuo Liu[1,2], Xinghua He[1,2], Yuzhan Yang[1,2] and Zhilin Yuan[1,2,*]

[1]State Key Laboratory of Tree Genetics and Breeding, Chinese Academy of Forestry, Beijing 100091, China

[2]Research Institute of Subtropical Forestry, Chinese Academy of Forestry, Hangzhou 311400, China

[3]State Key Laboratory of Ecological Pest Control for Fujian and Taiwan Crops, Fujian Agriculture and Forestry University, Fuzhou 350002, China

[4]Environmental Genomics, Christian-Albrechts University, 24118 Kiel, Germany

[5]Max Planck Fellow Group Environmental Genomics, Max Planck Institute for Evolutionary Biology, 24306 Plön, Germany

[6]Jiangsu Key Laboratory for Bioresources of Saline Soils, School of Wetlands, Yancheng Teachers University, Yancheng 224002, China

[7]Department of Agricultural and Food Sciences (DISTAL), University of Bologna, 40127 Bologna, Italy

[8]These authors contributed equally to this article.

***Correspondence: Eva H. Stukenbrock (estukenbrock@bot.uni-kiel.de), Zhilin Yuan (yuanzl@caf.ac.cn)**

https://doi.org/10.1016/j.xplc.2023.100672

ABSTRACT

Some fungal accessory chromosomes (ACs) may contribute to virulence in plants. However, the mechanisms by which ACs determine specific traits associated with lifestyle transitions along a symbiotic continuum are not clear. Here we delineated the genetic divergence in two sympatric but considerably variable isolates (16B and 16W) of the poplar-associated fungus *Stagonosporopsis rhizophilae*. We identified a ∼0.6-Mb horizontally acquired AC in 16W that resulted in a mildly parasitic lifestyle in plants. Complete deletion of the AC (Δ16W) significantly altered the fungal phenotype. Specifically, Δ16W was morphologically more similar to 16B, showed enhanced melanization, and established beneficial interactions with poplar plants, thereby acting as a dark septate endophyte. RNA sequencing (RNA-seq) analysis showed that AC loss induced the upregulation of genes related to root colonization and biosynthesis of indole acetic acid and melanin. We observed that the AC maintained a more open status of chromatin across the genome, indicating an impressive remodeling of *cis*-regulatory elements upon AC loss, which potentially enhanced symbiotic effectiveness. We demonstrated that the symbiotic capacities were non-host-specific through comparable experiments on *Triticum*– and *Arabidopsis*–fungus associations. Furthermore, the three isolates generated symbiotic interactions with a nonvascular liverwort. In summary, our study suggests that the AC is a suppressor of symbiosis and provides insights into the underlying mechanisms of mutualism with vascular plants in the absence of traits encoded by the AC. We speculate that AC-situated effectors and other potential secreted molecules may have evolved to specifically target vascular plants and promote mild virulence.

Key words: dark septate endophytes, effectors, lifestyle transition, root–fungus symbioses

Wei H., Zhong Z., Li Z., Zhang Y., Stukenbrock E.H., Tang B., Yang N., Baroncelli R., Peng L., Liu Z., He X., Yang Y., and Yuan Z. (2024). Loss of the accessory chromosome converts a pathogenic tree-root fungus into a mutualistic endophyte. Plant Comm. **5**, 100672.

INTRODUCTION

The ecological relevance of root-associated fungi in promoting plant health and fitness has been widely appreciated (Martin et al., 2017). In addition to mycorrhizal fungi, endophytic fungi

Published by the Plant Communications Shanghai Editorial Office in association with Cell Press, an imprint of Elsevier Inc., on behalf of CSPB and CEMPS, CAS.

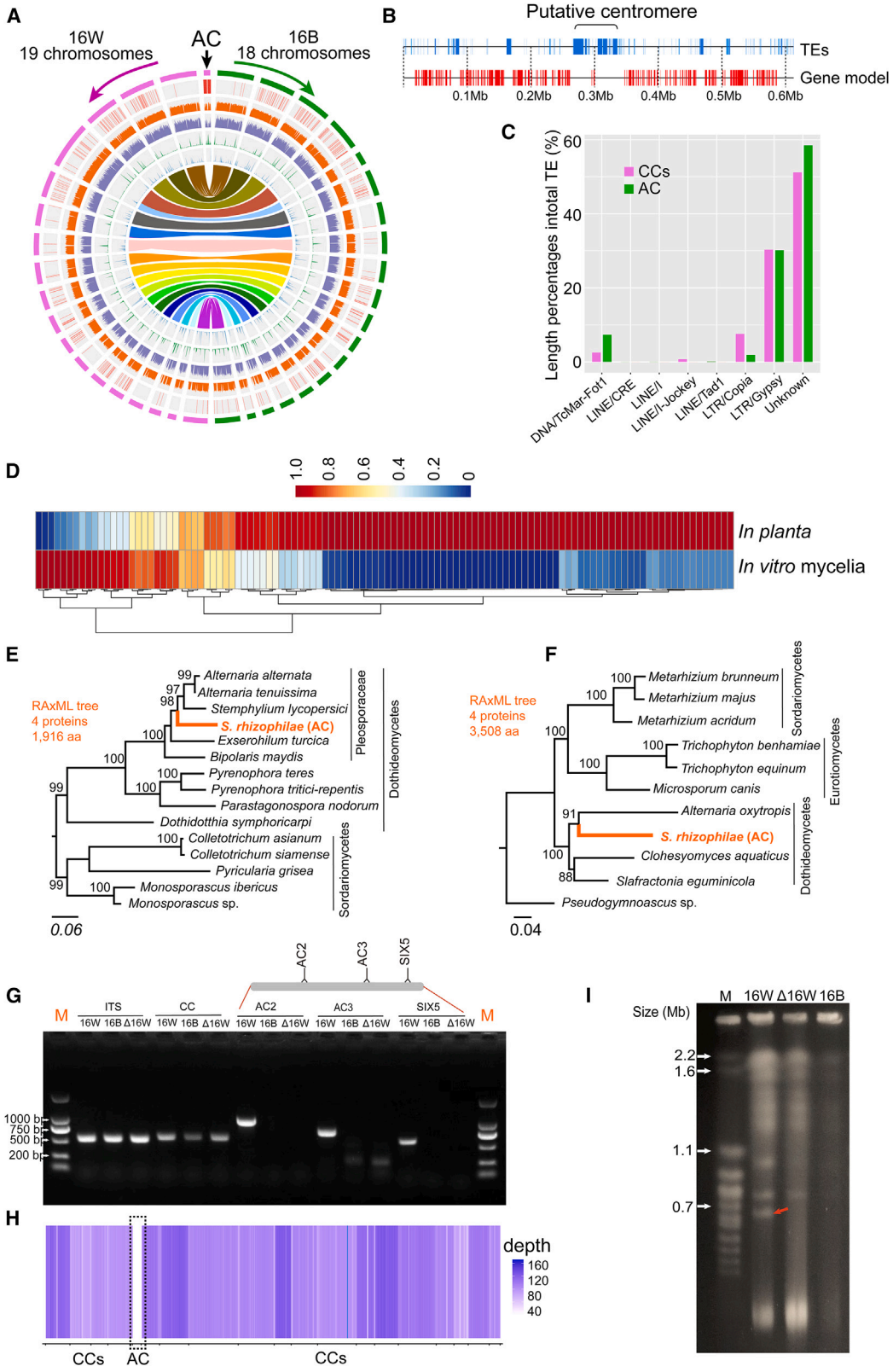

Figure 1. Identification of AC gain and loss in *S. rhizophilae* isolates.

(A) Circos plot showing chromosome-level synteny between the 16B and 16W isolates of *S. rhizophilae*. The ~0.6-Mb AC unique to 16W is indicated by a black arrow. The collinear regions between 16B and 16W are linked by same-colored lines. From inside to outside, the plot shows SNP/indel variation, repeat density, gene density, GC content, and unique genes.

(legend continued on next page)

also significantly influence the growth and survival of host plants (Rodriguez et al., 2009). The outcomes of root–fungus interactions can range from parasitism to mutualism (Redman et al., 2001; Zhou et al., 2021). Several studies have investigated the major genetic determinants of host specificity and lifestyle in these fungi and the corresponding mechanisms by which they interact with host plants. For example, *Colletotrichum magna* is a fungal pathogen that causes anthracnose in cucurbit plants, but a single gene mutation converts this pathogen into a non-pathogenic, endophytic mutualist that can protect plants from various diseases (Freeman and Rodriguez, 1993). A recent report described a metabolism gene cluster in *Colletotrichum tofieldiae* that modulated its lifestyle along the parasitic–mutualistic continuum in different environments (Hiruma et al., 2022). Several studies have reported that copy number variations (CNVs) may cause intraspecific genomic diversity in both arbuscular and ectomycorrhizal fungi and determine plant–mycorrhizal interactive outcomes and fungal lifestyle (Hortal et al., 2016; Mathieu et al., 2018; Dauphin et al., 2021). Furthermore, some plant pathogenic fungi harbor accessory chromosomes (ACs) that act as virulence/host specificity determinants (Ma et al., 2010; Habig et al., 2017). However, the mechanisms by which ACs determine specific traits associated with lifestyle switching in plant–fungus symbioses are not well characterized.

Recently, we reported the identification of two sympatric isolates of a novel fungus, *Stagonosporopsis rhizophilae* sp. nov. (Didymellaceae, Pleosporales, Ascomycota), with distinct phenotypes from the rhizosphere soils of *Populus deltoides* (Wei et al., 2021). However, the mechanisms underlying the phenotypic differences between the two isolates are unknown.

Therefore, in this study, we investigated whether the interactions between the two *S. rhizophilae* isolates and the poplar host varied, and we examined their potential genetic mechanisms. Specifically, we analyzed differences in melanization between the two isolates and their abilities to colonize roots and promote poplar growth. Broadly, we compared differences in genome structure between the isolates by evaluating chromosome-level genome assemblies. We also used a forward genetic approach to characterize the functional consequences of genomic alteration (i.e., AC loss). Finally, we investigated specific changes in transcriptional responses and genome-wide chromatin accessibility in relation to phenotypic variation and lifestyle transition.

RESULTS

Phylogenomic analysis shows that *S. rhizophilae* is a recently diverged species

We used telomere-to-telomere whole-genome assemblies of the two *S. rhizophilae* isolates, 16W and 16B, to investigate changes in genomic composition (Supplemental Table 1). These isolates were selected on the basis of their contrasting colony appearance. The genome sizes were 31.8 Mb for 16W and 31.3 Mb for 16B (Supplemental Figure 1). We annotated 11 488 and 11 381 protein-coding genes in 16W and 16B and demonstrated the completeness of the genome assemblies by recovering more than 99.6% of the 758 genes identified by Benchmarking Universal Single-Copy Orthologs (BUSCO) analysis using the fungi_odb10 gene sets (Simão et al., 2015). We also found that 8081 homologous protein families were shared between *S. rhizophilae*, *Stagonosporopsis tanaceti*, and *Stagonosporopsis vannaccii*, and 10 890 homologous protein families were shared between 16W and 16B (Supplemental Figure 1).

Next, we analyzed the phylogenomic relationships of *S. rhizophilae* with related taxa from the Didymellaceae, Pleosporaceae, and Didymosphaeriaceae families, most of which are pathogenic with the exception of two species of dark septate endophytes (DSEs), *Laburnicola rhizohalophila* (Yuan et al., 2020) and *Periconia macrospinosa* (Knapp et al., 2018). Both 16B and 16W were phylogenetically close to *S. tanaceti* with an estimated divergence time of 16.7 million years ago (mya) (a 95% confidence interval of 9.4–26.2 mya based on the general time reversible substitution model) (Supplemental Figure 1). Consistent with a previous report (Zhang et al., 2012), the phylogenomic analysis confirmed the phylogenetic position and evolutionary history of *Stagonosporopsis*.

Genome comparison reveals aneuploidy in *S. rhizophilae*

We compared the chromosome numbers of 16B and 16W using the complete telomere-to-telomere assemblies and identified 18 chromosomes in 16B and 19 chromosomes in 16W; 99.4% nucleotide identity and a high degree of genome co-linearity was observed between the 18 shared chromosomes of 16B and 16W, without any large-scale structural rearrangements (Figure 1A; Supplemental Figure 2). The smallest chromosome of 16W (Chr 19) was missing in 16B (Figure 1A). This result demonstrated aneuploidy in different isolates of *S. rhizophilae*.

(B) Diagram of transposable elements (TEs), gene models, and the putative centromere position on the AC.
(C) Comparison of TE content between the AC and core chromosomes (CCs).
(D) Analysis of a set of genes from the AC that showed significant differential expression between *in vitro* and *in planta* transcriptomes.
(E and F) Discordant phylogenetic relationships of proteins encoded by AC-resident genes. Maximum-likelihood trees were constructed from concatenated sequences of four genes that shared homologs in Pleosporaceae and other selected ascomycetous genera. Bootstrap values are indicated above the branches. Two individual trees were generated using four genes because the numbers of BlastP matches for the 136 AC-resident genes were low in the nr database.
(G) PCR amplification results of five loci confirm the presence of the AC in 16W and its absence in 16B and Δ16W. Three loci (AC2, AC3, and SIX5) across the two ends and central region of the AC were selected to confirm its complete loss. The fungal nuclear ribosomal internal transcribed spacer (ITS) and a CC locus were amplified as positive controls. The primer sequences are listed in Supplemental Table 7.
(H) Mapping of Illumina reads from Δ16W to the 16W genome. AC loss is confirmed by the lack of read coverage for the AC sequences in Δ16W.
(I) Electrophoretic karyotype of the AC. The chromosomal bands were separated by pulsed-field gel electrophoresis. A band of roughly 0.7 Mb present only in 16W is indicated by a red arrow. Chromosomes of *Schizosaccharomyces pombe* were used as markers.

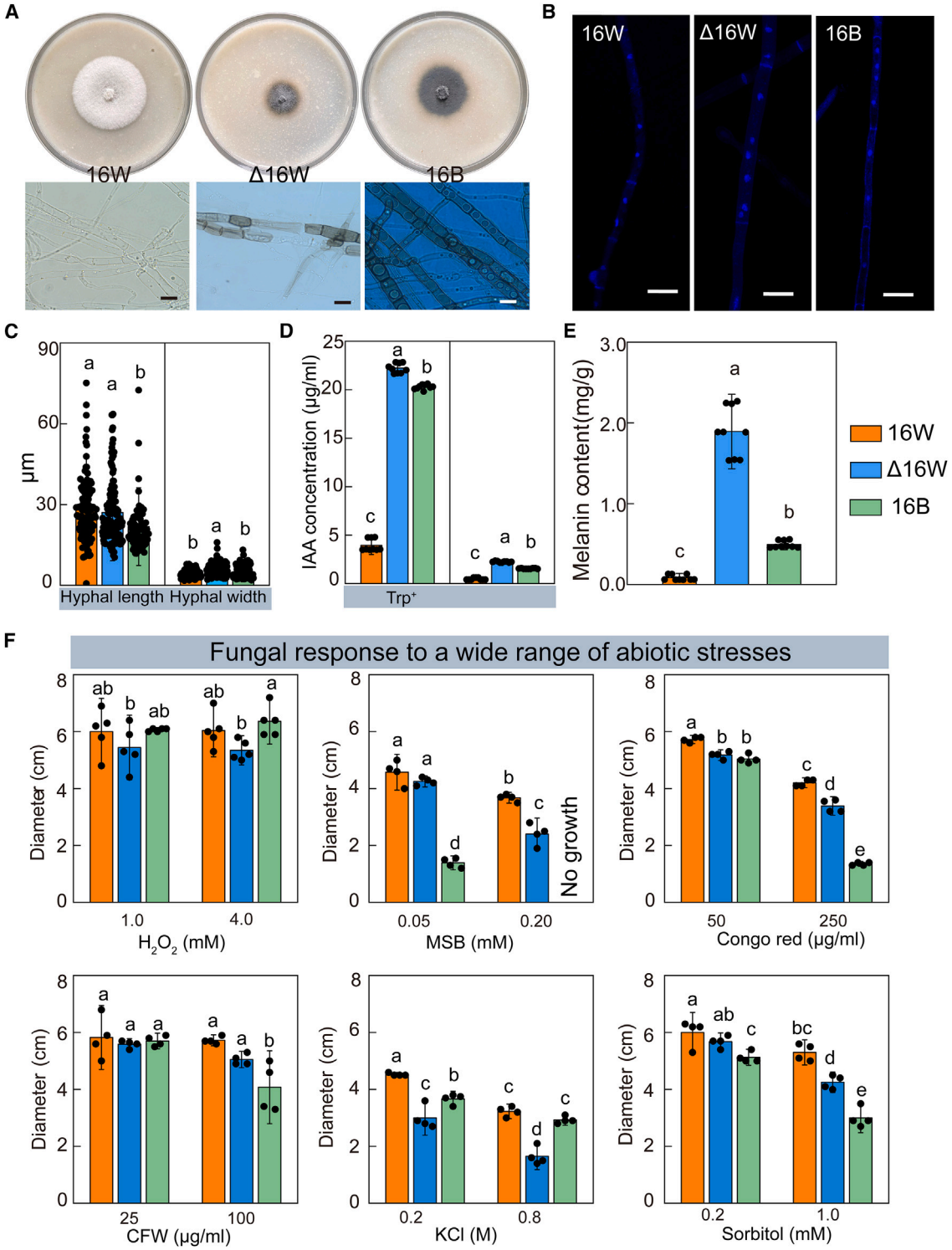

Figure 2. AC modulates the phenotypes, physiological traits (IAA and melanin), and tolerance of the *S. rhizophilae* isolates to stresses.

(A) Representative images show colony appearance and mycelial morphology of the three isolates (16W, Δ16W, and 16B). 16W shows hyaline mycelia, whereas Δ16W and 16B show melanized mycelia.

(B) Nuclear staining with DAPI reveals multiple nuclei in the hyphal cells of all three isolates.

(C) Length and width of hyphal cells from the three isolates.

(D) IAA production of the three isolates in the presence and absence of Trp.

(E) Melanin accumulation in mycelia of the three isolates.

(legend continued on next page)

Furthermore, this smallest chromosome showed a high percentage of repetitive sequences (12.5%), a low Guanine-Cytosine (GC) content (44%), a low gene density (233 genes/Mb), and chromosome-specific transposable elements (TEs). These features are hallmarks of ACs (Habig and Stukenbrock, 2020). By contrast, the remaining chromosomes showed a lower average percentage of repeated sequences (4.3%), a higher average GC content (50.9%), and a higher gene density (345 genes/Mb) (Figure 1B, 1C, and Supplemental Figure 3).

A total of 136 genes were located on Chr 19 and included two secondary metabolite biosynthetic clusters (type 1 polyketide synthase [T1PKS]) and a predicted open reading frame (ORF) that shared sequence similarities ranging from 34% to 36% with Secreted In Xylem 5 (SIX5) effectors from *Colletotrichum* and *Fusarium* species (E value < $2e^{-4}$). Gene Ontology (GO) term annotation demonstrated that most of the AC genes were associated with cellular, metabolic, and response-to-stimulus processes, the plasma membrane, and binding activity (Supplemental Figure 4). However, 11 genes lacked any GO term annotations.

Next, we analyzed the genes expressed from Chr 19. Transcriptomic data demonstrated that a higher number of genes were specifically expressed *in planta* than in the *in vitro* condition; 44 genes were significantly upregulated *in planta* compared with the *in vitro* mycelia (Figure 1D). The fragments per kilobase per million reads (FPKM) values of the five most highly expressed and upregulated genes ranged from 90 to 258. Mycelia grown *in planta* showed reduced expression of one *t1pks* and one *six5* gene and higher expression of another *t1pks* gene; 24 genes were not expressed in either condition.

Chr 19 is horizontally transferred and can be lost

We aligned the sequencing reads from Chr 19 to the genome sequences of 16B and its two closest relatives, *S. tanaceti* and *S. vannaccii*, and did not find any homologous regions. This suggested that Chr 19 was specific to 16W. To identify the origin of Chr 19, we performed a BlastP search of the non-redundant (nr) protein database and constructed phylogenetic trees based on amino acid sequences of four protein-coding genes from two separate datasets (Figures 1E and 1F). Our results suggested that proteins encoded by genes on Chr 19 were highly similar to those from *Alternaria*-related genera, and the gene tree topologies were distinct from that of the species tree (Supplemental Figure 1). Therefore, we postulated that Chr 19 was acquired by 16W through horizontal chromosome transfer from *Alternaria* or related taxa.

Previous studies in ascomycete fungi have demonstrated that ACs are unstable and can be lost during mitosis or meiosis without any adverse effect on basic fungal growth. We therefore investigated whether Chr 19 was essential for growth by treating 16W with carbendazim, a fungicide. We obtained a few fungicide-treated 16W colonies with unique phenotypic features, such as dark green colonies. We confirmed the complete deletion of Chr 19 using three parallel approaches. First, we designed three pairs of PCR primers to amplify specific genomic regions in Chr 19. We obtained negative results for all three PCRs in the fungicide-treated 16W strain and 16B but positive results for all the internal controls, including the nuclear ribosomal internal transcribed spacer (ITS) and a region located in one of the core chromosomes (CCs) (Figure 1G). Second, we sequenced the complete genome of the fungicide-treated 16W strain using the Illumina platform and mapped the reads to the 16W genome. The genome sequencing data showed that although reads from the fungicide-treated 16W strain aligned to the CCs, none of the reads aligned with Chr 19 reads from the wild-type 16W genome, thus demonstrating complete deletion of the AC in 16W (Δ16W) (Figure 1H). In addition, we identified only 25 SNPs and four indels in 18 CCs of Δ16W compared with 16W. This alleviated concerns regarding the presence of additional mutations during *in vitro* propagation and carbendazim treatment. Third, pulsed-field gel electrophoresis showed that the ∼0.6-Mb chromosomal band corresponding to Chr 19 in 16W was absent in Δ16W and 16B (Figure 1I). These data provide strong evidence that Chr 19 is completely deleted in the fungicide-treated 16W strain and absent in wild-type 16B.

AC loss reduces fungal fitness but increases synthesis of indole-3-acetic acid and melanin

Next, we analyzed whether the AC modulated phenotypic traits in *S. rhizophilae* by quantifying the morphological and biochemical differences among the wild-type (16B and 16W) and mutant (Δ16W) isolates. We observed significant differences among the three isolates in cell size, growth rate, colony appearance, and melanin and indole-3-acetic acid (IAA) production. The 16W colonies were white with thin and hyaline hyphae, whereas the 16B colonies were dark green in young cultures and black in older cultures, with heavily melanized hyphae (Figure 2A). The Δ16W colonies showed characteristics intermediate between those of 16B and 16W. DAPI staining revealed multiple nuclei (ranging from two to six) in each hyphal cell of all the three isolates (Figure 2B). Hyphal length and width differed significantly among the three isolates (one-way ANOVA, F = 6.62, P < 0.02, and F = 10.96, P < 0.001, respectively) (Figure 2C). However, Δ16W was occasionally unstable on PDA and showed chimeric white fertile patches and irregular or V-shaped sectors (Supplemental Figure 5). We attempted to stabilize the growth of Δ16W through single-hyphal-tip subculturing, but failed after two successive rounds of subculturing. We speculated that the chromosomal alteration in Δ16W likely resulted in dysregulation of genome architecture, accessibility, and gene expression, and that these were the causes of the phenotypic instability (Bruns and Barz, 2001; Orr et al., 2015). We therefore used the first subcultures that showed uniform colony appearance for further assays. We also created a second AC-deleted mutant line (Δ16W-1) to confirm the stability of the traits we observed (see below) in the AC-loss mutants (Supplemental Figure 6).

(F) Growth behaviors of the three isolates in response to a range of abiotic stresses, including oxidative stress (H_2O_2 and MSB), cell wall stress (Congo red and calcofluor white [CFW]), and osmotic stress (KCl and sorbitol). Different lowercase letters indicate significance levels. Error bars represent the SD of three replicates. Data were analyzed using ANOVA. Statistical significance was set to P < 0.05. Scale bars, 10 μm. MSB, menadione sodium bisulfite.

Biochemical assays demonstrated significant differences in IAA and melanin production among the three isolates (Figure 2D and 2E). IAA secretion was lower in 16W compared with Δ16W and 16B, whereas Δ16W secreted significantly higher amounts of IAA than 16B, especially in the presence of tryptophan (Trp) (Figure 2D). A similar pattern was observed for melanin accumulation, with significantly higher melanization in Δ16W and 16B and defective melanization in 16W (Figure 2E). The three isolates displayed variable biological behaviors when exposed to abiotic stresses (Figure 2F). In most cases, treatment with chemical stressors inhibited the growth of all three isolates, but the growth reduction was significantly lower in 16W than in 16B and Δ16W. This result suggested that 16W adapted to stressful environments better than Δ16W and 16B. Furthermore, Δ16W was less sensitive to oxidative stress induced by menadione sodium bisulfite (MSB) treatment and cell wall stress than 16B, but the latter was more tolerant to osmotic stress (KCl) and H_2O_2. An unexpected finding was that 16B was highly sensitive to MSB and completely inhibited at a concentration of 0.2 mM. This suggests that deletion or absence of AC significantly affects the ability of the fungus to thrive under stressful conditions. The abiotic stress responses of Δ16W-1 resembled those of Δ16W. One exception was that IAA production was lower in Δ16W-1 than in Δ16W (Supplemental Figure 6). Finally, we used the API-ZYM test and observed differences in the enzyme profiles among the three isolates. The activities of two proteolytic enzymes of particular interest, α-chymotrypsin and leucine arylamidase, were evident in Δ16W and/or 16B but absent in 16W (Supplemental Figure 7).

Loss of the AC increases the efficacy of symbiosis

Next, we analyzed whether the AC altered outcomes of the poplar–*S. rhizophilae* interaction. Three weeks after inoculation, we observed isolate-specific effects on poplar growth (Figure 3A). Poplar plants treated with 16W showed stunted growth and decreased leaf chlorophyll content compared with the control group (Supplemental Figure 8), but they did not display any apparent disease symptoms. This suggested that 16W was most likely to be saprotrophic or mildly parasitic on the poplar plants. By contrast, the number of adventitious and lateral roots was significantly increased in Δ16W- and 16B-colonized poplar plants compared with those treated with or without 16W inoculation (Figure 3A). The increased root development correlated with higher IAA production in both Δ16W and 16B. 16W was defective in penetrating the poplar roots and inhabited only the root surface, whereas both Δ16W and 16B showed increased colonization levels (Figure 3B). Specifically, around 7 days post inoculation (dpi), we observed that hyphae of Δ16W and 16B had directly entered the root epidermal cells. After 1 month of plant growth, trypan blue staining confirmed that 16B had initiated the formation of microsclerotium-like structures in the cortical cells that were composed of clusters of irregularly shaped, melanized hyphal cells (Figure 3B). The colonization pattern of Δ16W was very similar to that of 16B, although we did not observe fully developed microsclerotium-like structures. Overall, these infection structures were reminiscent of DSEs. Wheat germ agglutinin (WGA) staining further confirmed that hyphae of 16W were limited to the root surface, whereas hyphae of Δ16W and 16B showed intensive penetration and proliferation along the epidermal and cortical cells (Figure 3B).

We next measured *in situ* ROS (H_2O_2) production as a read-out of the plant response to fungal invasion during a 72-h post-inoculation time course. We observed a strong dark brownish-red precipitate in 16B-colonized roots from the first time point (16 h post-inoculation) onward, demonstrating elevated H_2O_2 production upon 16B colonization (Figure 3C and Supplemental Figure 8). The Δ16W-colonized roots showed lower 3,3′-diaminobenzidine (DAB) staining during the early stage but intense staining after 32 h post inoculation (Figure 3C and Supplemental Figure 8). 16W inoculation did not stimulate any H_2O_2 production in roots at 16 or 32 h post inoculation, and relatively weak staining was observed at later time points. We speculated that extensive colonization and micro-sclerotial development required remodeling of root cell walls and was therefore correlated with H_2O_2 production.

We also observed a delay in the appearance of wilting symptoms after exposure to salinity stress in the 16B-inoculated plants. Kaplan–Meier survival analysis demonstrated increased survival of the 16B-treated poplar seedlings compared with the controls after 1 month of salinity stress, although this difference was not statistically significant (Supplemental Figure 8). By contrast, 16W-inoculated plants were more susceptible to saline-induced stress and showed signs of salt injury. However, the Δ16W-colonized plants did not show reduced damage from salinity stress and were comparable to uninoculated plants (Supplemental Figure 8).

AC-independent symbiotic stabilization is observed in a liverwort

To further investigate the regulatory role of ACs in plant–fungal symbioses, we extended our study to a wider range of plants. We chose three non-host plants for parallel inoculation assays: wheat, *Arabidopsis*, and the liverwort *Marchantia polymorpha*. The results were consistent with our findings for the poplar–fungus association. Both Δ16W and 16B significantly promoted the growth of wheat and *Arabidopsis* compared with corresponding controls, whereas 16W reduced the fitness of wheat and *Arabidopsis* (Figure 3A). This result suggests that the plant–*S. rhizophilae* interaction model is largely conserved across monocot and dicot lineages. However, we also observed a trend toward parasitism when comparing poplar and *Arabidopsis*, because 16W showed markedly enhanced virulence on *Arabidopsis*. By contrast, all three isolates significantly improved the growth of *M. polymorpha*, although the growth-stimulating effects of 16W did not surpass those of Δ16W and 16B. Microscopy observations revealed that the fungal colonization patterns in the three non-host plants resembled that in the poplar–fungus association (Supplemental Figure 9). Moreover, fungal-colonized thalli were significantly greener (with more chlorophyll) than those of controls (Figure 3A). This result points to increased chlorophyll biosynthesis in *M. polymorpha* inoculated with the three isolates. These two lines of experimental evidence demonstrate that the AC does not have negative effects on the nonvascular liverwort. We repeated the plant inoculation experiments with Δ16W-1 and demonstrated that, in most cases, it had a significant positive effect on plant growth (Supplemental Figure 6).

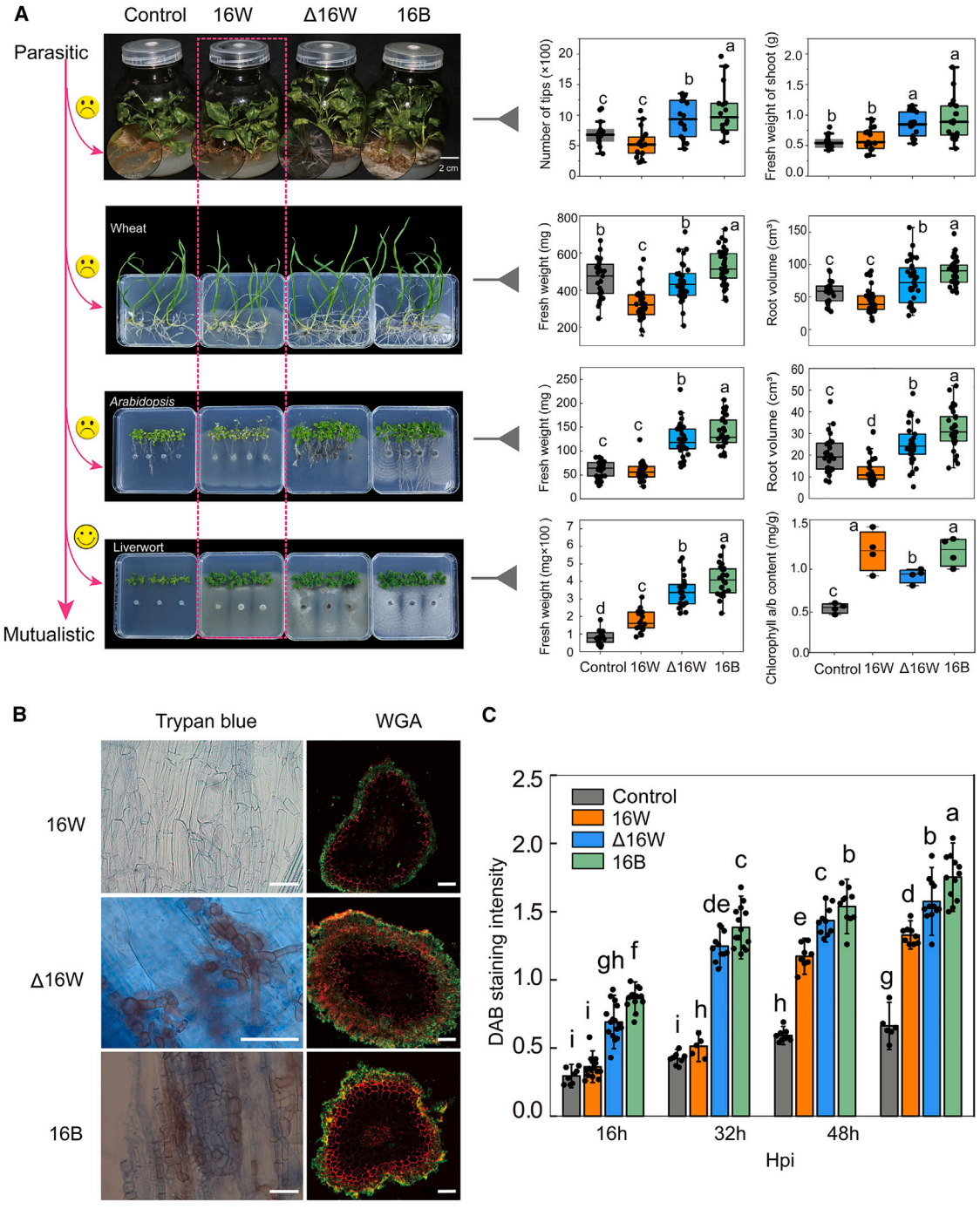

Figure 3. Contrasting interaction outcomes in associations of *S. rhizophilae with* vascular and nonvascular plants.

(A) Plant biomass, root development, and chlorophyll content (for liverwort) increased upon Δ16W and 16B inoculation, although better performance was observed in the 16B-inoculated plants. For plant–16W interactions, a trend toward mutualism was recorded during a shift from vascular plants (poplar, wheat, and *Arabidopsis*) to the nonvascular liverwort. The plant growth status in each inoculation test was analyzed by ANOVA.

(B) Staining of poplar root cross sections and squash mounts demonstrates the root colonization patterns of the three isolates. Δ16W and 16B triggered development of microsclerotium-like structures and melanized hyphae in the roots, and the hyphae extended into the inner cortical cells. By contrast, 16W only colonized the root surface and showed no penetration. Root cell walls were stained with phosphatidylinositol (PI), and fungal hyphae were labeled with wheat germ agglutinin (WGA). Microscopy observations were performed on roots at 1 month after colonization. Scale bars, 50 μm. Microscopy examinations of fungal colonization in roots (rhizoids for liverwort) of the three non-host plants are presented in Supplemental Figure 9.

(C) DAB staining intensity at four time points in poplar roots inoculated with the three isolates. Hpi, hours post-inoculation. Error bars represent SDs of the replicates. Different lowercase letters indicate significant differences. Data were analyzed by one-way ANOVA. Statistical significance was set to $P < 0.05$.

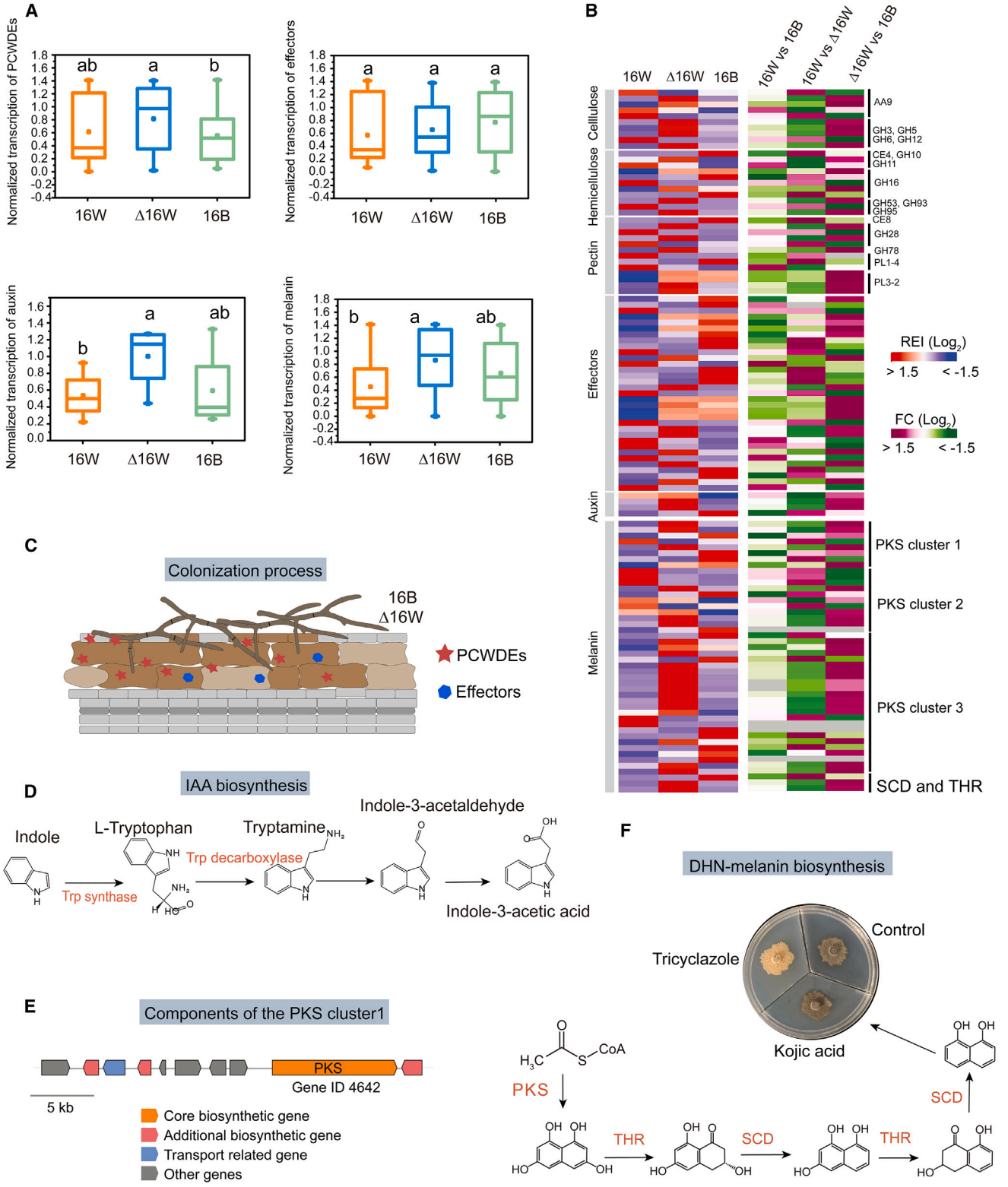

Figure 4. AC regulates expression of fungal genes related to PCWDEs, manipulation of plant immunity, and biosynthesis of IAA and melanin.

(A) Bar plots show the average normalized expression values for genes encoding PCWDEs, effectors, and IAA and melanin biosynthetic enzymes. Statistical differences were calculated using the Mann–Whitney U-test. The significance level ($P < 0.05$) is indicated by different lowercase letters.

(legend continued on next page)

Loss of the AC induces genome-wide transcriptional remodeling and is related to lifestyle transition

We next investigated whether loss or absence of the AC was associated with changes in gene expression levels on a genome-wide scale. We first compared the gene expression patterns of *in vitro*-grown mycelia from Δ16W, 16W, and 16B using RNA sequencing (RNA-seq) (Supplemental Table 2; Supplemental Figure 10). Approximately one-fifth of the genes (ranging from 15.9% to 28.6%) were differentially expressed in the three pairwise comparisons ($|\log_2 FC| \geq 2$, false discovery rate $q < 0.05$) (Supplemental Figure 11). For example, 16W showed significant upregulation of 1509 genes and downregulation of 1305 genes compared with Δ16W (Supplemental Figure 11). Overall, we documented a high degree of global transcriptional divergence between isolates with and without the AC (16W vs. 16B) and between the AC-containing isolate and the AC-deleted mutant (16W vs. Δ16W).

We subsequently compared specific gene expression patterns linked to lifestyle-related and mutualistic traits. This work was performed under *in vitro* conditions. We found that 16B and Δ16W were generally characterized by a concerted and isolate-specific upregulation of effectors and plant cell-wall-degrading enzymes (PCWDEs), both of which are critical for the onset of successful root infection and the attenuation of plant immune responses (Figure 4A–4C). Broadly, genes targeting cellulose, hemicellulose, and pectin exhibited a moderate increase in expression levels in Δ16W compared with 16W, whereas effector-related transcripts tended to show higher expression levels in 16B (Figure 4A), although differences in average expression levels among the three isolates did not reach the level of statistical significance. This result suggests that relatively low expression of effectors and PCWDEs in 16W could be responsible for its poor root colonization ability, although more detailed analyses of gene expression at different time points *in planta*, in particular at early and middle stages of plant colonization, will be required to validate the results.

Next, we analyzed the transcript levels of genes that modulated IAA and melanin production by searching for homologs involved in dihydroxynaphthalene (DHN)-melanin biosynthesis (PKSs, scytalone dehydratase, and tetrahydroxynaphthalene [THN] reductase) (Yuan et al., 2021) and Trp-dependent IAA biosynthesis (Trp synthase and Trp decarboxylase) (Jahn et al., 2021) (Figure 4D–4F). The expression levels of most genes involved in DHN-melanin biosynthesis and Trp-dependent IAA biosynthesis were increased by three-fold in Δ16W compared with 16W (Figure 4D–4F). This probably explained the higher melanin production in Δ16W, as shown in the *in vitro* assay. Therefore, de-repression of melanin biosynthetic clusters increased melanization in Δ16W and facilitated the development of melanized microsclerotium-like structures in roots. We also observed significantly higher expression of genes involved in IAA biosynthesis in Δ16W (Figure 4A). Together, these data highlight mechanisms by which AC loss promotes the transition from a parasitic to a mutualistic lifestyle.

The AC regulates the genome-wide landscape of chromatin accessibility

We next asked whether AC loss altered chromatin accessibility, which could account for the genome-wide transcriptional changes. We performed assay for transposase-accessible chromatin with high-throughput sequencing (ATAC-seq) to profile genome-wide accessible chromatin regions where active *cis*-regulatory elements were enriched (Figure 5A). We used the same growth conditions and age of fungal material as for the RNA-seq analysis to compare the two datasets. Features of the ATAC-seq data are shown in Supplemental Table 3 and Supplemental Figures 12 and 13. Most of the accessible regions were enriched between 2 kb upstream of the transcription start site and 2 kb downstream of the transcription end site (Supplemental Figure 13). In all libraries, the insert size distribution of fragments displayed a predominant peak corresponding to nucleosome-free regions (<100 bp) and did not show periodicity, except for the 16B libraries, which showed a mono-nucleosome protected region (150–250 bp) and a di-nucleosome protected region (>250 bp) (Supplemental Figure 13).

We identified 4041 and 5552 accessible chromatin regions in 16B and 16W, respectively (Supplemental Table 4). However, only 1578 accessible chromatin regions were recovered in Δ16W, demonstrating that AC loss significantly inhibited chromatin openness at the genome-wide level (Figure 5B). Next, we investigated the link between changes in chromatin accessibility and alterations in gene expression by integrating the ATAC-seq data with the RNA-seq data. We first linked changes in gene expression with alterations in chromatin accessibility and observed a weak but significant positive correlation between differentially expressed genes (DEGs) and differentially accessible regions (DARs) (Supplemental Figure 14). This correlation may have been skewed because we observed a number of genes with lower chromatin openness being upregulated or vice versa (Supplemental Table 5). Specifically,

(B) Expression levels of various genes of interest in the three isolates. PCWDE-encoding genes are classified into three groups: those involved in the degradation of cellulose, hemicellulose, and pectin. Predicted effectors with differential expression were also selected. Most transcripts of genes involved in IAA and melanin biosynthesis (three PKS clusters, 1,3,4-trihydroxynaphthalene reductase [THR], and scytalone dehydratase [SCD]) were upregulated in Δ16W and 16B. Z score–transformed expression data are visualized in the heatmaps. The color key from blue to red indicates low to high gene expression. Gene expression fold changes (green, downregulated; violet, upregulated) were calculated for each pairwise comparison.
(C) Schematic illustration of fungal colonization in the roots, which was facilitated by increased activities of PCWDEs and effectors in 16B and Δ16W.
(D) The Trp-dependent IAA biosynthetic pathway in fungi. Two key enzymes (Trp synthase and Trp decarboxylase) identified in our study are highlighted in bold orange.
(E) Gene expression analysis of PKS cluster 1. The core *pks* gene (ID 4642) was highly expressed in 16B, together with more accessible chromatin in the upstream region of this gene (see Figure 5D).
(F) Gene expression analysis of genes encoding enzymes involved in the DHN-melanin biosynthetic pathway (highlighted in bold orange). Melanin biosynthesis inhibitors (tricyclazole and kojic acid, 50 μg ml^{-1}) were used to confirm that *S. rhizophilae* synthesizes DHN-melanin but not dihydroxyphenyalanine (DOPA) melanin. All RNA-seq data were generated from 3-day-old mycelia grown *in vitro*.

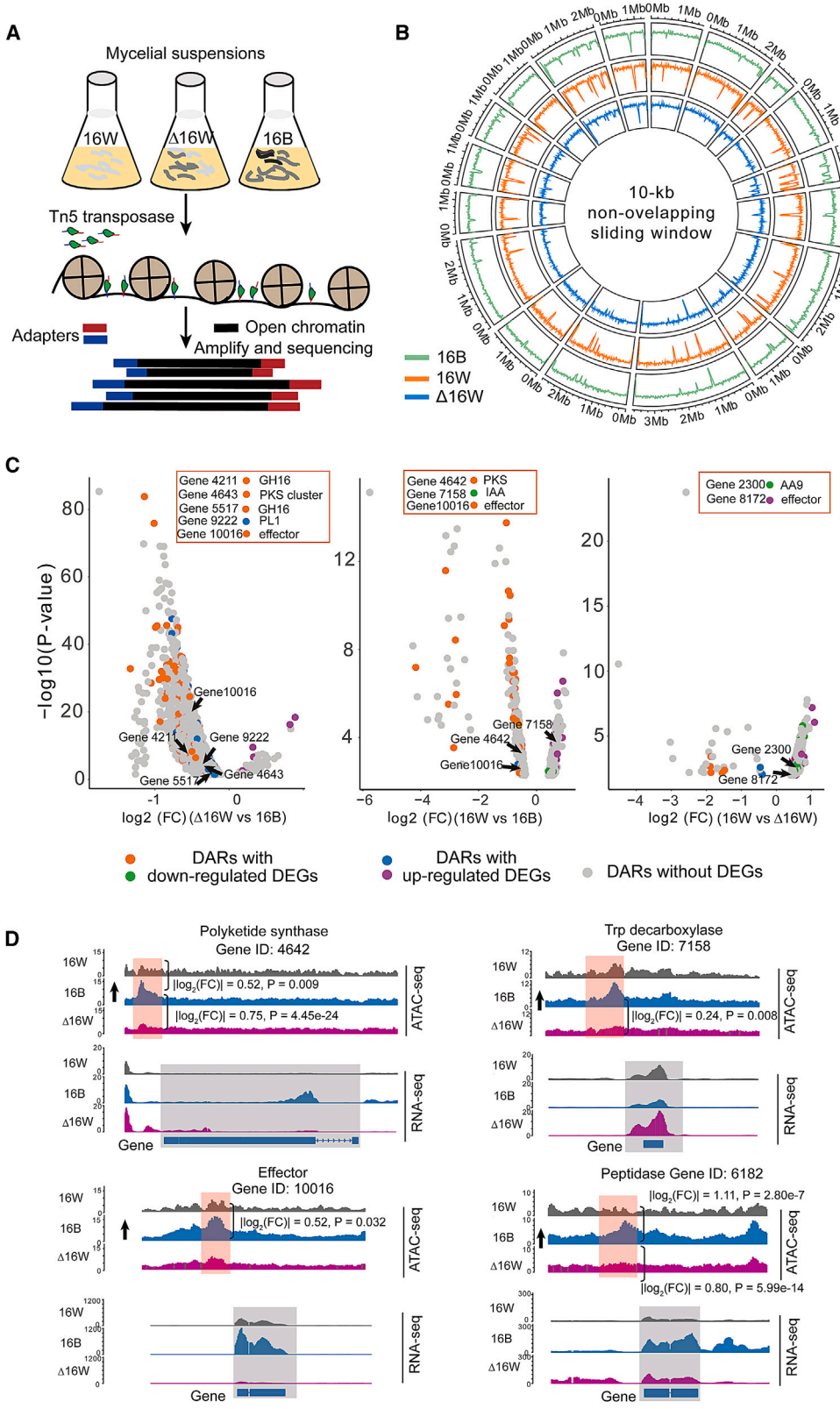

Figure 5. Significant effect of the AC on genome-wide chromatin accessibility and correlation between DARs and DEGs.

(A) Schematic representation of the ATAC-seq workflow for the three isolates of *S. rhizophilae*.

(B) Genome-wide distribution of ATAC-seq signals over 10-kb non-overlapping sliding windows analyzed using Bedtools v2.29.2. The outside ring indicates the length of each chromosome. In brief, 16W shows more open chromatin sites, whereas Δ16W and 16B show lower chromatin accessibility.

(legend continued on next page)

the majority of DARs were not associated with DEGs (Figure 5C). Several genes of interest that showed increased expression levels also demonstrated shifts from open to closed or from closed to open conformation (Figure 5C). For example, the three top upregulated genes in 16B, peptidase (gene ID: 6182), PKS (gene ID: 4642), and effector (gene ID: 10016), were associated with the greatest increase in chromatin accessibility compared with 16W (Figure 5D). However, a gene encoding Trp decarboxylase (gene ID: 7158) showed higher expression in Δ16W and displayed a more closed chromatin status compared with 16B. Thus, it appears likely that the major DEGs are not only associated with increased or decreased chromatin accessibility but also influenced by other factors, such as specific gene regulatory modules or pathways.

Identification of potential footprints of transcription factors encoded by the AC

In addition to harboring potential effectors and secondary metabolite clusters, ACs also encode transcription factors (TFs), which play an essential role in gene regulation (Yang et al., 2020). We hypothesized that close crosstalk between the AC and CCs was mediated by TFs from the AC. We therefore aimed to identify candidate AC-resident TFs and their potential binding motifs in the CCs. We identified three TFs on the AC: IXR1, ECM22, and GAL4 (E values = 0). ECM22 and GAL4 encode TFs with Zn (II)2-Cys6 zinc-finger domains and are essential for ergosterol (Yang et al., 2015) and galactose metabolism (Zhao et al., 2011), respectively, whereas the high-mobility group domain in IXR1 is often associated with response to oxidative stress in fungi (Mota et al., 2021). We identified their corresponding predicted TF-binding motifs in CCs (JASPAR accessions MA0292.1, ECM22; MA0299.1, GAL4; MA0323.1, IXR1; Supplemental Figure 14) and observed typical TF-binding footprints in GAL4 and IXR1. GO enrichment analysis revealed that the IXR1-binding genes were enriched in signal transduction and cellular communication (Supplemental Figure 15).

DISCUSSION

Implications of vascular and nonvascular plant–fungus interactions: The yin and yang of ACs

The main finding of this study is the discovery of an AC in *S. rhizophilae*. ACs were first identified in the plant pathogenic fungus *Nectria haematococca* (Miao et al., 1991). Since then, one to 11 ACs have been reported in 26 fungal species (Leclair et al., 1996; Akamatsu et al., 1999; D'Ambrosio et al., 2017; Plaumann and Koch, 2020; Bertazzoni et al., 2021; Zaccaron et al., 2022). To the best of our knowledge, this is the first study to report the existence of an AC in the Didymellaceae family.

The regulatory roles of ACs in fungal pathogenicity are a matter of debate. The prevailing hypothesis suggests that ACs are associated with increased virulence because they are rich in genes encoding effectors and secondary metabolite gene clusters (Ma et al., 2010; Wang et al., 2019; Plaumann and Koch, 2020). In the pathogenic fungus *Colletotrichum higginsianum*, loss of one AC did not alter growth on artificial media but resulted in a pronounced decline in infection of host leaves. Interestingly, loss of a second AC did not affect the growth phenotype or virulence of the fungus (Plaumann et al., 2018). Furthermore, in *Fusarium oxysporum* f. sp. lycopersici (Fol 4287), complete loss of chromosome 12, 14, or 15 did not significantly alter *in vitro* growth and development (Vlaardingerbroek et al., 2016). By contrast, loss of an AC increased pathogenicity of *Zymoseptoria tritici* but did not adversely affect fitness (Habig et al., 2017). The biocontrol *Fusarium* isolate Fo47 was also reported to contain an AC (Brader et al., 2017; Guo et al., 2021). Therefore, ACs may perform various functions apart from their role in modulating virulence (Soyer et al., 2018). Despite these pioneering studies, the underlying mechanisms by which ACs regulate symbiotrophic interactions are still unknown. Broadly, our study revealed that Δ16W, generated by loss of the AC from 16W, showed characteristics similar to those of 16B (a wild-type isolate that did not harbor the AC), including the DSE phenotype and increased IAA production. This finding indicates the presence of an active biochemical and physiological mechanism for establishment of mutualism in the absence of the AC. These phenotypes were still stable in the *Triticum*– and *Arabidopsis*–fungus associations, suggesting an evolutionarily conserved role for the AC in suppressing symbiosis. Furthermore, 16B conferred salinity tolerance to poplar plants, but these effects were not observed with Δ16W or 16W. This result implies the presence of an additional as-yet-unidentified mechanism to account for this defensive mutualism. Importantly, we found that the AC orchestrated a mutualistic lifestyle in the *M. polymorpha*–fungus association, indicating that 16W expressed mutualism in a host-dependent manner. This finding was contrary to a recent study in which the Fo47 isolate benefited angiosperm hosts but still caused disease symptoms in *M. polymorpha* (Redkar et al., 2022). We thus argue that the AC is functional in vascular plants but compromised in the liverwort. This may be linked to the fact that the SIX5-like effector and other secreted molecules encoded in the AC emerged after the divergence of nonvascular and vascular plants and may have evolved to specifically target vascular lineages.

Our AC gene model was identical to the Fo47 isolate, in which the AC-resident genes are significantly enriched for cell signaling and not for virulence (Guo et al., 2021). Therefore, we wanted to determine the implications of this fungus for AC-mediated adaptive evolution. The presence of a few genes that encode members of protein kinase families and G protein-coupled receptors suggested the potential adaptive nature of the AC. Our data contrast with previous reports in which a low number of ACs did not significantly affect fungal fitness (Möller et al., 2018; Chen et al., 2022) because we recorded increased melanization and reduced fitness in Δ16W. This suggests that the AC is required

(C) Volcano plot showing all differentially accessible peaks. The orange and green dots represent DARs associated with downregulated DEGs; blue and violet dots represent DARs associated with upregulated DEGs. The gray dots represent regions with significantly reduced or increased chromatin accessibility but without DEGs. Genes of interest are indicated by black arrows and listed with functional annotations.

(D) Genome browser tracks of ATAC-seq (red) and RNA-seq (gray) signals for four representative DEGs. The peak diagram shows the relationship between genes in open chromatin regions and gene expression levels. Gene symbols are labeled for the corresponding loci. The $\log_2$ fold changes in chromatin accessibility and the corresponding *P* values are shown. The black arrows indicate a more open chromatin status in 16B.

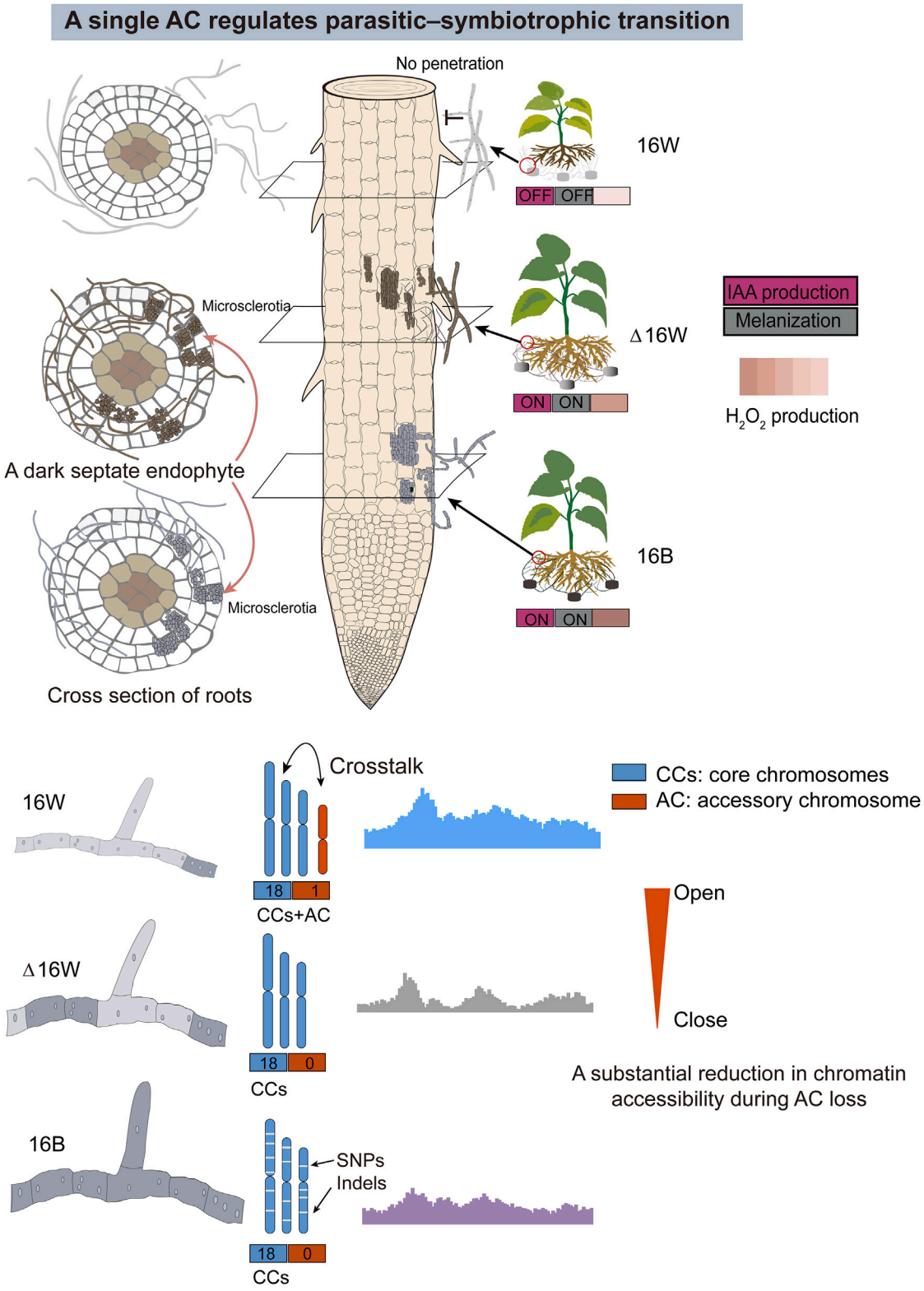

Figure 6. Conceptual diagram highlighting AC-mediated dynamic poplar–fungus interactions.
Both the AC-deleted (Δ16W) and natural AC-absent (16B) isolates act as DSEs and confer a key mutualistic trait for aiding poplar plant growth. Specifically, lack of a single AC increases melanization and IAA production, as shown by significant upregulation of genes related to melanin and IAA biosynthesis. Results also show significant changes in transcripts of genes encoding PCWDEs and effectors, which enable Δ16W and 16B to attenuate the plant immune response and colonize the root cortical cells. On the other hand, growth of 16W is confined to the root surface, probably because of

(legend continued on next page)

for response to external stresses. Previous studies have shown that melanin plays a critical role in conferring resilience to chemical and abiotic stresses (Griffiths et al., 2018). However, our results showed that increased melanization did not promote survival in 16B and Δ16W. Recent reports have also suggested that oxidative tolerance is not always associated with melanin regulation (Francisco et al., 2020; Malo et al., 2020). Therefore, our results suggest a tradeoff paradigm in which the AC provides a specific advantage to the fungus but attenuates its mutualistic traits in interactions with vascular plants. In the future, a broader sampling of pathogenic and beneficial *Stagonosporopsis* isolates will be required to better understand the distribution and functional role of ACs within this genus.

Origin of the AC and active interplay between AC and CCs

It is still challenging to understand how 16W acquired the AC. In our study, genomic analysis did not show any orthologs of AC-associated genes in the 18 CCs or other species in Didymellaceae. However, 93% of the AC-resident genes showed high similarity to genes from Pleosporaceae taxa or other genetically distant ascomycete fungi. A previous study (Ma et al., 2010) reported that some AC-resident genes from *F. oxysporum* were homologous to those of other *Fusarium* species, whereas the remaining genes were similar to those of unrelated species. Together, our data suggest horizontal acquisition of the AC from *Alternaria*-related genera.

Our study showed that AC loss was sufficient to increase melanization of 16W, thereby demonstrating the functional relevance of the AC and its dynamic crosstalk with the CCs (Habig and Stukenbrock, 2020; Yang et al., 2020; Gan et al., 2021). Although ACs are considered highly heterochromatic (Habig et al., 2017; Soyer et al., 2018), our study showed that 48% and 73% of AC-resident genes were expressed during *in vitro* mycelial growth and *in planta* colonization, respectively. This suggests their potential to affect the expression of genes from CCs. The activation of genes related to melanin and IAA biosynthesis after AC loss supports this notion. However, the possible effects of AC-resident TFs on the expression of CC-resident genes are not known and warrant investigation. Moving forward, thanks to the chromatin immunoprecipitation sequencing technique, we may have the opportunity to reveal how the three TFs orchestrate specific gene expression in the CCs, as shown by significant up-regulation of ECM22 and GAL4 transcripts *in planta*. Equally important, functional complementation through re-introduction of the AC to Δ16W should be a priority in future research to strictly demonstrate the roles of the AC.

Regulation of gene expression: Beyond chromatin accessibility

Changes in mRNA levels can be due to specific *cis*-acting sequences and the degree of chromatin accessibility. There are usually some overlaps between DEGs and DARs (Merrill et al., 2022). Our data support this notion, despite the weak Pearson coefficients observed. However, when we take a closer look at these relationships, the situation seems to be complicated. As shown in Supplemental Table 5 and Figure 5C, only a small proportion of DEGs showed significant open or closed chromatin accessibility. This discrepancy can be explained in two ways. First, transcription of these unique DEGs may be regulated by transcriptional repressors (Miao et al., 2021) or gene regulatory modules (Cirino et al., 2020; Jenull et al., 2020; Zhong et al., 2021) that may be located far from the gene loci (Ackermann et al., 2016). In our study, the highly expressed genes, which were correlated with traits of interest in Δ16W, were not associated with significant changes in chromatin status. Second, chromatin changes may precede gene expression changes. The euchromatin state is necessary for gene expression and can be detected from ATAC-seq data but may not be evident in the RNA-seq data (Jia et al., 2018; Chen et al., 2021). Further experiments are necessary to confirm these possibilities.

Our study showed that AC loss resulted in a significant reduction in chromatin accessibility. Although the mechanistic details are not yet known, this finding was consistent with a previous report in which deletion of a ∼200-kb segment from the mouse X chromosome resulted in loss of 62% of ATAC-seq peaks (Giorgetti et al., 2016). A plausible reason for decreased chromatin accessibility may be changes in DNA methylation (Zhong et al., 2021), as inferred from identification of a putative homolog of *O*-methyltransferase (gene ID: 7573) in the AC. Another intriguing question that remains unexplained is the clear transcriptional differences between Δ16W and 16B. It is plausible that these differences are due to minor genomic differences in the 18 CCs. Careful scrutiny of the two genomes did not reveal a wealth of genetic variations. We identified only 33 non-synonymous SNPs in Δ16W when mapping reads to the 16B genome (Supplemental Table 6). We also identified 315 deletions and 151 insertions (<100 bp) that caused frameshift mutations in 30 genes. We further detected a relatively large deletion event (∼79.4 kb), but significant CNVs were not present (see the supplemental information). This deletion region contained six unknown genes. We therefore conclude that a combination of the AC and subtle genetic differences in the CCs directly affect gene expression or cause perturbations in *cis*-regulatory regions, which may cause major phenotypic changes.

In summary, we describe a novel AC in a tree-root-associated ascomycete. The AC helps to maximize fungal fitness under various abiotic stresses and may regulate complicated root–fungus interactions, as shown by AC-independent symbiotic stabilization in a liverwort. In other words, the AC may define a host-dependent lifestyle of the fungus as being either mutualistic or parasitic. A working model for the AC-mediated changes in mutualistic interactions is shown in Figure 6. Future studies will be required to investigate the roles of ACs in the origin, diversity, and functions of DSEs, which are ecologically critical non-mycorrhizal root guilds.

large-scale silencing of these genes. The *in vivo* root H_2O_2 production shows that development of microsclerotium-like structures is accompanied by increased but tightly controlled H_2O_2 production to stabilize the mutualism. Meanwhile, the AC maintains a more open chromatin status across the genome, and its deletion or absence is associated with a larger number of closed chromatin sites. This scenario indicates an impressive remodeling of *cis*-regulatory elements upon AC loss. Thus, the AC—together with minor genetic variations in the CCs (SNPs and indels)—contributes to extensive transcriptional remodeling, phenotypic plasticity, and interaction outcomes (mildly parasitic versus mutualistic) in vascular plants.

METHODS

Genome sequencing, assembly, and annotation

We used long-read sequencing to generate highly contiguous assemblies and improved assembly accuracy using a polishing pipeline with Illumina short reads. The detailed protocol has been described elsewhere (He and Yuan, 2021). Telomeric tandem repeat six-nucleotide sequences of TTAGGG (or the complementary sequence, AATCCC) were identified at both ends of almost all scaffolds, indicating complete chromosomes. We combined *de novo*, homology, and transcriptome-based strategies to predict protein-coding genes. When identifying TEs, we used the *de novo* prediction tools RepeatModeler v1.0.11 and LTR_FINDER v1.0.6.

Phylogenomic analysis and molecular dating

We identified a total of 2369 one-to-one orthologs for phylogenomic reconstruction. These single-copy orthologous sequences were aligned with MUSCLE (Edgar, 2004). The unambiguously aligned conserved blocks were extracted with Gblocks v0.91b (Castresana, 2000). The concatenated alignment was used to create a Bayesian inference of phylogeny in MrBayes v3.1.2. For molecular dating, the Hysteriales divergence time at 90–213 mya (Liu et al., 2017) and the Pleosporales divergence time at 148–274 mya (www.timetree.org) were chosen as two calibration points. We inferred the divergence time of each tree node using the Bayesian Markov-chain Monte Carlo tree (MCMCTree) package in PAML v4.9 with the GTR nucleotide substitution model.

In silico annotation of effectors and CAZymes

The secretome was predicted with the web-based program SECRETOOL (http://genomics.cicbiogune.es/SECRETOOL/Secretool.php), and EffectorP 3.0 was used to identify candidate effectors (Sperschneider and Dodds, 2022). To identify the total CAZyme repertoire of *S. rhizophilae*, we used the dbCAN2 web-based meta server v2.0.1 for CAZyme annotation (Zhang et al., 2018). To annotate secreted CAZymes, we determined the presence of signal peptides using SignalP 5.0 (https://services.healthtech.dtu.dk/service.php?SignalP-5.0).

Macro-synteny analysis

Syntenic blocks were detected with the MCScanX toolkit (https://github.com/wyp1125/MCScanX) (Wang et al., 2012). Pairwise macro-synteny plots were drawn with Circos v0.69 (Krzywinski et al., 2009).

Generation and confirmation of AC-loss mutants

We used the fungicide carbendazim to induce AC loss as described previously (Habig et al., 2017), with some modifications, and used three approaches to confirm complete loss. The methods and procedures are given in the supplemental information and Supplemental Table 7.

Profiling of fungal physiological traits

Using the AC mutant, we evaluated the extent to which AC loss contributes to phenotypic variation and symbiotic interactions. Phenotypic analyses were performed, including analyses of auxin (IAA) and melanin production *in vitro* and various abiotic stress tests. These functional traits could, to a large extent, reflect the ecology and genetic differences of fungi. More detail is provided in the supplemental information.

Plant and fungal growth conditions and inoculation test design

We used micro-propagated *Populus* seedlings for the inoculation test. Under gnotobiotic growth systems, we measured an array of plant phenotypic and physiological traits affected by fungal colonization. We also characterized the growth of three other plants (wheat, *Arabidopsis*, and liverwort) in response to fungal colonization to determine whether the plant–fungus interactions were evolutionarily conserved across a wide range of plant lineages. See more details in the supplemental information.

RNA-seq and ATAC-seq data analysis

We generated fungal transcriptome data under the *in vitro* growth condition. Fungal mycelia were harvested from PDB liquid cultures after 3 days. The fresh mycelium was immediately frozen with liquid nitrogen and homogenized for RNA extraction. Three independent biological replicates were performed for each isolate. Note that *in planta* fungal transcriptomes were also analyzed from 16W-colonized roots in order to compare AC-associated gene expression patterns between *in vitro* and *in planta* conditions.

In parallel, we used an ATAC-seq assay to link chromatin accessibility with transcriptional regulation on a genome-wide scale (Buenrostro et al., 2013). The three isolates were cultured under the same conditions for RNA-seq and ATAC-seq (Jenull et al., 2021). To minimize bias, three independent biological replicates were performed for each isolate. More details on RNA-seq and ATAC-seq library construction, sequencing, and data analysis are provided in the supplemental information.

Statistical analysis

Prior to statistical analyses, all phenotypic and physiological datasets were tested for normality and homogeneity of variance with the Shapiro–Wilk test and Levene's test, respectively. All phenotypic and physiological datasets (fungal growth under different conditions, melanin and IAA production, and plant growth status) were subjected to one-way analysis of variance in SPSS Statistics v20. When a significant F test result was obtained at $P = 0.05$, the analysis of variance was followed by Tukey's *post hoc* test at $P \leq 0.05$. All data were expressed as mean values with SDs.

DATA AND CODE AVAILABILITY

The genome sequences and assemblies of 16B and 16W have been deposited in the Genome Assembly and Annotations (GWH) of the National Genomics Data Center (NGDC) under accession numbers GWHDRIK00000000 and GWHDRIJ00000000. Raw reads from transcriptomes and ATAC-seq were also deposited in the Genome Sequence Archive (GSA) at the NGDC under accession numbers CRA012076, CRA012077, and CRA012079.

SUPPLEMENTAL INFORMATION

Supplemental information is available at *Plant Communications Online*.

FUNDING

This work was financially supported by the National Key Research and Development Program of China (2022YFD2201900) and the National Natural Science Foundation of China (no. 31722014).

AUTHOR CONTRIBUTIONS

Y.Z.L. conceived the study. Y.Z.L., Z.H.Z., E.H.S., and B.P.T. designed the experiments. H.S.W., Z.F.L., N.N.Y., Y.W.Z., L.P., Z.L., X.H.H., and Y.Z.Y. carried out the experiments and performed the data analysis. Z.H.Z. and R.B. interpreted the data. Y.Z.L. wrote the manuscript. E.H.S., Z.H.Z., and R.B. reviewed and edited the manuscript.

ACKNOWLEDGMENTS

We are grateful to Dr. Asen Daskalov (Université de Bordeaux) for careful reading of the paper and for his comments and detailed suggestions. We thank other lab members for technical support. No conflict of interest is declared.

Received: February 17, 2023
Revised: June 1, 2023
Accepted: August 4, 2023
Published: August 9, 2023

REFERENCES

Ackermann, A.M., Wang, Z., Schug, J., Naji, A., and Kaestner, K.H. (2016). Integration of ATAC-seq and RNA-seq identifies human alpha cell and beta cell signature genes. Mol. Metabol. **5**:233–244. https://doi.org/10.1016/j.molmet.2016.01.002.

Akamatsu, H., Taga, M., Kodama, M., Johnson, R., Otani, H., and Kohmoto, K. (1999). Molecular karyotypes for *Alternaria* plant pathogens known to produce host-specific toxins. Curr. Genet. **35**:647–656. https://doi.org/10.1007/s002940050464.

Bertazzoni, S., Jones, D.A.B., Phan, H.T., Tan, K.C., and Hane, J.K. (2021). Chromosome-level genome assembly and manually-curated proteome of model necrotroph *Parastagonospora nodorum* Sn15 reveals a genome-wide trove of candidate effector homologs, and redundancy of virulence-related functions within an accessory chromosome. BMC Genom. **22**:382. https://doi.org/10.1186/s12864-021-07699-8.

Brader, G., Compant, S., Vescio, K., Mitter, B., Trognitz, F., Ma, L.J., and Sessitsch, A. (2017). Ecology and genomic insights into plant-pathogenic and plant-nonpathogenic endophytes. Annu. Rev. Phytopathol. **55**:61–83. https://doi.org/10.1146/annurev-phyto-080516-035641.

Bruns, R., and Barz, W. (2001). Studies on cell number and nuclei in spores and on ploidy level in *Ascochyta rabiei* isolates. J. Phytopathol. **149**:253–258. https://doi.org/10.1046/j.1439-0434.2001.00613.x.

Buenrostro, J.D., Giresi, P.G., Zaba, L.C., Chang, H.Y., and Greenleaf, W.J. (2013). Transposition of native chromatin for fast and sensitive epigenomic profiling of open chromatin, DNA-binding proteins and nucleosome position. Nat. Methods **10**:1213–1218. https://doi.org/10.1038/nmeth.2688.

Castresana, J. (2000). Selection of conserved blocks from multiple alignments for their use in phylogenetic analysis. Mol. Biol. Evol. **17**:540–552. https://doi.org/10.1093/oxfordjournals.molbev.a026334.

Chen, D., Parker, T.M., Bhat-Nakshatri, P., Chu, X., Liu, Y., Wang, Y., and Nakshatri, H. (2021). Nonlinear relationship between chromatin accessibility and estradiol-regulated gene expression. Oncogene **40**:1332–1346. https://doi.org/10.1038/s41388-020-01607-2.

Chen, J., Birchler, J.A., and Houben, A. (2022). The non-Mendelian behavior of plant B chromosomes. Chromosome Res. **30**:229–239. https://doi.org/10.1007/s10577-022-09687-4.

Cirino, A., Aurigemma, I., Franzese, M., Lania, G., Righelli, D., Ferrentino, R., Illingworth, E., Angelini, C., and Baldini, A. (2020). Chromatin and transcriptional response to loss of TBX1 in early differentiation of mouse cells. Front. Cell Dev. Biol. **8**, 571501. https://doi.org/10.3389/fcell.2020.571501.

D'Ambrosio, U., Alonso-Lifante, M.P., Barros, K., Kovařík, A., Mas de Xaxars, G., and Garcia, S. (2017). B-chrom: a database on B-chromosomes of plants, animals and fungi. New Phytol. **216**:635–642. https://doi.org/10.1111/nph.14723.

Dauphin, B., de Freitas Pereira, M., Kohler, A., Grigoriev, I.V., Barry, K., Na, H., Amirebrahimi, M., Lipzen, A., Martin, F., Peter, M., et al. (2021). Cryptic genetic structure and copy-number variation in the ubiquitous forest symbiotic fungus *Cenococcum geophilum*. Environ. Microbiol. **23**:6536–6556. https://doi.org/10.1111/1462-2920.15752.

Edgar, R.C. (2004). MUSCLE: Multiple sequence alignment with high accuracy and high throughput. Nucleic Acids Res. **32**:1792–1797. https://doi.org/10.1093/nar/gkh340.

Francisco, C.S., Zwyssig, M.M., and Palma-Guerrero, J. (2020). The role of vegetative cell fusions in the development and asexual reproduction of the wheat fungal pathogen *Zymoseptoria tritici*. BMC Biol. **18**:99. https://doi.org/10.1186/s12915-020-00838-9.

Freeman, S., and Rodriguez, R.J. (1993). Genetic conversion of a fungal plant pathogen to a nonpathogenic, endophytic mutualist. Science **260**:75–78. https://doi.org/10.1126/science.260.5104.75.

Gan, P., Hiroyama, R., Tsushima, A., Masuda, S., Shibata, A., Ueno, A., Kumakura, N., Narusaka, M., Hoat, T.X., Narusaka, Y., et al. (2021). Telomeres and a repeat-rich chromosome encode effector gene clusters in plant pathogenic *Colletotrichum* fungi. Environ. Microbiol. **23**:6004–6018. https://doi.org/10.1111/1462-2920.15490.

Giorgetti, L., Lajoie, B.R., Carter, A.C., Attia, M., Zhan, Y., Xu, J., Chen, C.J., Kaplan, N., Chang, H.Y., Heard, E., et al. (2016). Structural organization of the inactive X chromosome in the mouse. Nature **535**:575–579. https://doi.org/10.1038/nature18589.

Griffiths, S.A., Cox, R.J., Overdijk, E.J.R., Mesarich, C.H., Saccomanno, B., Lazarus, C.M., de Wit, P.J.G.M., and Collemare, J. (2018). Assignment of a dubious gene cluster to melanin biosynthesis in the tomato fungal pathogen *Cladosporium fulvum*. PLoS One **13**, e0209600. https://doi.org/10.1371/journal.pone.0209600.

Guo, L., Yu, H., Wang, B., Vescio, K., Delulio, G.A., Yang, H., Berg, A., Zhang, L., Edel-Hermann, V., Steinberg, C., et al. (2021). Metatranscriptomic comparison of endophytic and pathogenic *Fusarium*-Arabidopsis interactions reveals plant transcriptional plasticity. Mol. Plant Microbe Interact. **34**:1071–1083. https://doi.org/10.1094/MPMI-03-21-0063-R.

Habig, M., Quade, J., and Stukenbrock, E.H. (2017). Forward genetics approach reveals host genotype-dependent importance of accessory chromosomes in the fungal wheat pathogen *Zymoseptoria tritici*. mBio **8**:e01919-17. https://doi.org/10.1128/mBio.01919-17.

Habig, M., and Stukenbrock, E.H. (2020). Origin, function, and transmission of accessory chromosomes. In Genetics and Biotechnology, J.P. Benz and K. Schipper, eds., *Vol. 2*. The Mycota (Springer). https://doi.org/10.1007/978-3-030-49924-2_2.

He, X., and Yuan, Z. (2021). Near-chromosome-level genome assembly of the dark septate endophyte *Laburnicola rhizohalophila*: a model for investigating root-fungus symbiosis. Genome Biol. Evol. **13**, evab026. https://doi.org/10.1093/gbe/evab026.

Hiruma, K., Aoki, S., Utami, Y.D., Okamoto, M., Kawamura, N., Nakamura, M., Ohmori, Y., Sugita, R., Tanoi, K., Sato, T., et al. (2022). A fungal secondary metabolism gene cluster enables mutualist-pathogen transition in root endophyte *Colletotrichum tofieldiae*. Preprint at bioRxiv. https://doi.org/10.1101/2022.07.07.499222.

Hortal, S., Powell, J.R., Plett, J.M., Simonin, A., and Anderson, I.C. (2016). Intraspecific competition between ectomycorrhizal *Pisolithus microcarpus* isolates impacts plant and fungal performance under elevated CO_2 and temperature. FEMS Microbiol. Ecol. **92**:fiw113. https://doi.org/10.1093/femsec/fiw113.

Jahn, L., Hofmann, U., and Ludwig-Müller, J. (2021). Indole-3-acetic acid is synthesized by the endophyte *Cyanodermella asteris* via a tryptophan-dependent and-independent way and mediates the interaction with a non-host plant. Int. J. Mol. Sci. **22**:2651. https://doi.org/10.3390/ijms22052651.

Jenull, S., Mair, T., Tscherner, M., Penninger, P., Zwolanek, F., Silao, F.G.S., de San Vicente, K.M., Riedelberger, M., Bandari, N.C., Shivarathri, R., et al. (2021). The histone chaperone HIR maintains chromatin states to control nitrogen assimilation and fungal virulence. Cell Rep. **36**, 109406. https://doi.org/10.1016/j.celrep.2021.109406.

Jenull, S., Tscherner, M., Mair, T., and Kuchler, K. (2020). ATAC-seq identifies chromatin landscapes linked to the regulation of oxidative stress in the human fungal pathogen *Candida albicans*. J. Fungi **6**:182. https://doi.org/10.3390/jof6030182.

Jia, G., Preussner, J., Chen, X., Guenther, S., Yuan, X., Yekelchyk, M., Kuenne, C., Looso, M., Zhou, Y., Teichmann, S., et al. (2018). Single cell RNA-seq and ATAC-seq analysis of cardiac progenitor cell transition states and lineage settlement. Nat. Commun. **9**:4877. https://doi.org/10.1038/s41467-018-07307-6.

Knapp, D.G., Németh, J.B., Barry, K., Hainaut, M., Henrissat, B., Johnson, J., Kuo, A., Lim, J.H.P., Lipzen, A., Nolan, M., et al. (2018). Comparative genomics provides insights into the lifestyle and reveals functional heterogeneity of dark septate endophytic fungi. Sci. Rep. **8**:6321. https://doi.org/10.1038/s41598-018-24686-4.

Krzywinski, M., Schein, J., Birol, I., Connors, J., Gascoyne, R., Horsman, D., Jones, S.J., and Marra, M.A. (2009). Circos: an information aesthetic for comparative genomics. Genome Res. **19**:1639–1645. https://doi.org/10.1101/gr.092759.109.

Leclair, S., Ansan-Melayah, D., Rouxel, T., and Balesdent, M. (1996). Meiotic behaviour of the minichromosome in the phytopathogenic ascomycete *Leptosphaeria maculans*. Curr. Genet. **30**:541–548. https://doi.org/10.1007/s002940050167.

Liu, J.K., Hyde, K.D., Jeewon, R., Phillips, A.J.L., Maharachchikumbura, S.S.N., Ryberg, M., Liu, Z.Y., and Zhao, Q. (2017). Ranking higher taxa using divergence times: a case study in Dothideomycetes. Fungal Divers. **84**:75–99. https://doi.org/10.1007/s13225-017-0385-1.

Ma, L.J., van der Does, H.C., Borkovich, K.A., Coleman, J.J., Daboussi, M.J., Di Pietro, A., Dufresne, M., Freitag, M., Grabherr, M., Henrissat, B., et al. (2010). M. Rep, Comparative genomics reveals mobile pathogenicity chromosomes in *Fusarium*. Nature **464**:367–373. https://doi.org/10.1038/nature08850.

Malo, M.E., Schultzhaus, Z., Frank, C., Romsdahl, J., Wang, Z., and Dadachova, E. (2020). Transcriptomic and genomic changes associated with radioadaptation in *Exophiala dermatitidis*. Comput. Struct. Biotechnol. J. **19**:196–205. https://doi.org/10.1016/j.csbj.2020.12.013.

Martin, F.M., Uroz, S., and Barker, D.G. (2017). Ancestral alliances: Plant mutualistic symbioses with fungi and bacteria. Science **356**, eaad4501. https://doi.org/10.1126/science.aad4501.

Mathieu, S., Cusant, L., Roux, C., and Corradi, N. (2018). Arbuscular mycorrhizal fungi: intraspecific diversity and pangenomes. New Phytol. **220**:1129–1134. https://doi.org/10.1111/nph.15275.

Merrill, C.B., Montgomery, A.B., Pabon, M.A., Shabalin, A.A., Rodan, A.R., and Rothenfluh, A. (2022). Harnessing changes in open chromatin determined by ATAC-seq to generate insulin-responsive reporter constructs. BMC Genom. **23**:399. https://doi.org/10.1186/s12864-022-08637-y.

Miao, V.P., Covert, S.F., and VanEtten, H.D. (1991). A fungal gene for antibiotic resistance on a dispensable ("B") chromosome. Science **254**:1773–1776. https://doi.org/10.1126/science.1763326.

Miao, W., Ma, Z., Tang, Z., Yu, L., Liu, S., Huang, T., Wang, P., Wu, T., Song, Z., Zhang, H., et al. (2021). Integrative ATAC-seq and RNA-seq analysis of the longissimus muscle of Luchuan and Duroc pigs. Front. Nutr. **8**, 742672. https://doi.org/10.3389/fnut.2021.742672.

Möller, M., Habig, M., Freitag, M., and Stukenbrock, E.H. (2018). Extraordinary Genome Instability and Widespread Chromosome Rearrangements During Vegetative Growth. Genetics **210**:517–529. https://doi.org/10.1534/genetics.118.301050.

Mota, M.N., Martins, L.C., and Sá-Correia, I. (2021). The identification of genetic determinants of methanol tolerance in yeast suggests differences in methanol and ethanol toxicity mechanisms and candidates for improved methanol tolerance engineering. J. Fungi **7**:90. https://doi.org/10.3390/jof7020090.

Orr, B., Godek, K.M., and Compton, D. (2015). Aneuploidy. Curr. Biol. **25**:R538–R542. https://doi.org/10.1016/j.cub.2015.05.010.

Plaumann, P.L., and Koch, C. (2020). The many questions about mini chromosomes in *Colletotrichum* spp. Plants **9**:641. https://doi.org/10.3390/plants9050641.

Plaumann, P.L., Schmidpeter, J., Dahl, M., Taher, L., and Koch, C. (2018). A dispensable chromosome is required for virulence in the hemibiotrophic plant pathogen *Colletotrichum higginsianum*. Front. Microbiol. **9**:1005. https://doi.org/10.3389/fmicb.2018.01005.

Redkar, A., Gimenez Ibanez, S., Sabale, M., Zechmann, B., Solano, R., and Di Pietro, A. (2022). *Marchantia polymorpha* model reveals conserved infection mechanisms in the vascular wilt fungal pathogen *Fusarium oxysporum*. New Phytol. **234**:227–241. https://doi.org/10.1111/nph.17909.

Redman, R.S., Dunigan, D.D., and Rodriguez, R.J. (2001). Fungal symbiosis from mutualism to parasitism: who controls the outcome, host or invader? New Phytol. **151**:705–716. https://doi.org/10.1046/j.0028-646x.2001.00210.x.

Rodriguez, R.J., White, J.F., Jr., Arnold, A.E., and Redman, R.S. (2009). Fungal endophytes: diversity and functional roles. New Phytol. **182**:314–330. https://doi.org/10.1111/j.1469-8137.2009.02773.x.

Simão, F.A., Waterhouse, R.M., Ioannidis, P., Kriventseva, E.V., and Zdobnov, E.M. (2015). BUSCO online supplementary information: assessing genome assembly and annotation completeness with single-copy orthologs. Bioinformatics **31**:3210–3212. https://doi.org/10.1093/bioinformatics/btv351.

Soyer, J.L., Balesdent, M.H., Rouxel, T., and Dean, R.A. (2018). To B or not to B: a tale of unorthodox chromosomes. Curr. Opin. Microbiol. **46**:50–57. https://doi.org/10.1016/j.mib.2018.01.012.

Sperschneider, J., and Dodds, P.N. (2022). EffectorP 3.0: prediction of apoplastic and cytoplasmic effectors in fungi and oomycetes. Mol. Plant Microbe Interact. **35**:146–156. https://doi.org/10.1094/MPMI-08-21-0201-R.

Vlaardingerbroek, I., Beerens, B., Rose, L., Fokkens, L., Cornelissen, B.J.C., and Rep, M. (2016). Exchange of core chromosomes and horizontal transfer of lineage-specific chromosomes in *Fusarium oxysporum*. Environ. Microbiol. **18**:3702–3713. https://doi.org/10.1111/1462-2920.13281.

Wang, M., Fu, H., Shen, X.X., Ruan, R., Rokas, A., and Li, H. (2019). Genomic features and evolution of the conditionally dispensable chromosome in the tangerine pathotype of *Alternaria alternata*. Mol. Plant Pathol. **20**:1425–1438. https://doi.org/10.1111/mpp.12848.

Wang, Y., Tang, H., Debarry, J.D., Tan, X., Li, J., Wang, X., Lee, T.H., Jin, H., Marler, B., Guo, H., et al. (2012). *MCScanX*: a toolkit for detection and evolutionary analysis of gene synteny and collinearity. Nucleic Acids Res. **40**:e49. https://doi.org/10.1093/nar/gkr1293.

Wei, H., He, X., Riccardo, B., Yang, Y., and Yuan, Z. (2021). *Stagonosporopsis rhizophilae* sp. nov. (Didymellaceae, Pleosporales), a new rhizospheric soil fungus associated with *Populus deltoides* Marsh. Phytotaxa **491**:23–34. https://doi.org/10.11646/phytotaxa.00.0.0.

Yang, H., Tong, J., Lee, C.W., Ha, S., Eom, S.H., and Im, Y.J. (2015). Structural mechanism of ergosterol regulation by fungal sterol transcription factor Upc2. Nat. Commun. **6**:6129. https://doi.org/10.1038/ncomms7129.

Yang, H., Yu, H., and Ma, L.J. (2020). Accessory chromosomes in *Fusarium oxysporum*. Phytopathology **110**:1488–1496. https://doi.org/10.1094/PHYTO-03-20-0069-IA.

Yuan, Z., Druzhinina, I.S., Gibbons, J.G., Zhong, Z., Van de Peer, Y., Rodriguez, R.J., Liu, Z., Wang, X., Wei, H., Wu, Q., et al. (2021). Divergence of a genomic island leads to the evolution of melanization in a halophyte root fungus. ISME J. **15**:3468–3479. https://doi.org/10.1038/s41396-021-01023-8.

Yuan, Z., Druzhinina, I.S., Wang, X., Zhang, X., Peng, L., and Labbé, J. (2020). Insight into a highly polymorphic endophyte isolated from the roots of the halophytic seepweed *Suaeda salsa: Laburnicola rhizohalophila* sp. nov. (Didymosphaeriaceae, Pleosporales). Fungal Biol. **124**:327–337. https://doi.org/10.1016/j.funbio.2019.10.001.

Zhang, H., Yohe, T., Huang, L., Entwistle, S., Wu, P., Yang, Z., Busk, P.K., Xu, Y., and Yin, Y. (2018). DbCAN2: a meta server for automated carbohydrate-active enzyme annotation. Nucleic Acids Res. **46**:W95–W101. https://doi.org/10.1093/nar/gky418.

Zhang, Y., Crous, P.W., Schoch, C.L., and Hyde, K.D. (2012). Pleosporales. *Fungal Divers.* **53**:1–221. https://doi.org/10.1007/s13225-011-0117-x.

Zhao, C., Waalwijk, C., de Wit, P.J.G.M., van der Lee, T., and Tang, D. (2011). EBR1, a novel Zn_2Cys_6 transcription factor, affects virulence and apical dominance of the hyphal tip in *Fusarium graminearum*. Mol. Plant Microbe Interact. **24**:1407–1418. https://doi.org/10.1094/MPMI-06-11-0158.

Zhong, Z., Feng, S., Duttke, S.H., Potok, M.E., Zhang, Y., Gallego-Bartolomé, J., Liu, W., and Jacobsen, S.E. (2021). DNA methylation-linked chromatin accessibility affects genomic architecture in *Arabidopsis*. Proc. Natl. Acad. Sci. USA **118**, e2023347118. https://doi.org/10.1073/pnas.2023347118.

Zhou, L., Li, X., Kotta-Loizou, I., Dong, K., Li, S., Ni, D., Hong, N., Wang, G., and Xu, W. (2021). A mycovirus modulates the endophytic and pathogenic traits of a plant associated fungus. ISME J. **15**:1893–1906. https://doi.org/10.1038/s41396-021-00892-3.